Structural and Multidisciplinary Optimization (2021) 63:2955–2967
https://doi.org/10.1007/s00158-020-02829-4

INDUSTRIAL APPLICATION PAPER

Multi-objective optimal sizing of energy dissipative steel cushions for longitudinal loading

Ahmet Güllü[1] · Seda Göktepe Körpeoğlu[2] · Elif Sıla Selek Kılıçarslan[3]

Received: 23 July 2020 / Revised: 30 October 2020 / Accepted: 18 December 2020 / Published online: 2 January 2021

Abstract

Contemporary approach in earthquake engineering tends to dissipate some part of seismic energy by additional fuses. Owing to its easy-to-produce and plug-and-play characteristics, energy dissipative steel cushion (SC) can be a prominent candidate to serve this purpose. Since its closed form design equations are already available in the literature, seismic performance and energy dissipative characteristics of SC might be improved by optimal sizing. Hence, distinct mathematical optimization techniques, namely sequential quadratic programming, gradient-based method, and Lagrange multiplier method, are employed. Results of the optimization techniques are evaluated through experimentally verified finite element analyses. Consequently, some geometric dimension ratios are provided for the optimal sizing of SCs. Comparisons between the optimization studies yielded that the gradient-based method requires fewer function evaluations to converge while the Lagrange multiplier method with a Hessian produces more accurate results.

Keywords Multi-objective optimization · Optimal sizing · Energy dissipator · Metallic damper · Finite element analysis

1 Introduction

Conventionally, seismic energy imparted to a structure is dissipated by deformations of the structural members and/or joints. However, recent applications require dissipating significant part of the seismic energy by energy dissipative fuse elements to enhance seismic performance of the structures. It was stated in the literature that top and/or story displacements, accelerations, and shear forces can be reduced reasonably by the additional damping supplied by the energy dissipators (Aiken 1996; Sadek et al. 1996; Soong and Spencer Jr. 2002). Many types of energy dissipation systems that benefit from distinct mechanisms such as friction (Dal Lago et al. 2017), yielding of metals (Zhou et al. 2019), viscosity of liquids (Sonmez et al. 2013), and metallurgical properties of lead (Soydan et al. 2014, 2018, 2020) have been implemented into many kinds of structures.

Energy dissipative steel cushions (SCs) which are produced from mild steel have been proven to be an efficient alternative for seismic energy dissipation (Ozkaynak et al. 2014, 2018; Yuksel et al. 2018; Güllü et al. 2019). Initially, SCs were developed for the connection of precast reinforced concrete (RC) cladding panels to the main building (Safecladding 2015; Colombo et al. 2016). However, application areas of the SCs were not limited with it (Karadoğan et al. 2019). SCs were utilized in the longitudinal direction to improve seismic behavior of frame-type structures experimentally by Güllü et al. (2018) and numerically by Güllü et al. (2018) and Ozkaynak (2018). In these studies, SCs were found to be judiciously efficient for retrofitting or seismic performance enhancement purposes. Nevertheless, the efficiency of SCs may be improved by sizing its geometrical dimensions through optimization techniques which aim possible best solution. These techniques have been widely applied to the energy dissipative elements to improve their efficiency by optimal sizing or optimal placement throughout the structure in the literature.

Responsible Editor: Axel Schumacher

✉ Ahmet Güllü
ahmet.gullu@gedik.edu.tr

[1] Department of Civil Engineering, Istanbul Gedik University, Istanbul, Turkey

[2] Department of Mathematical Engineering, Yıldız Technical University, Istanbul, Turkey

[3] Department of Mechanical Engineering, Istanbul Gedik University, Istanbul, Turkey

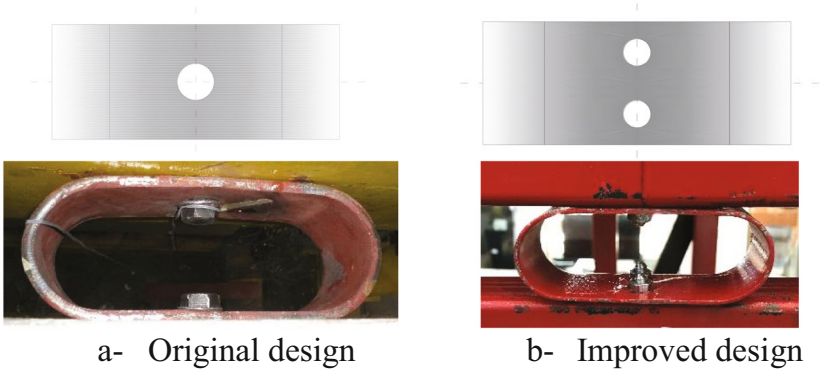

Fig. 1 **a**, **b** Energy dissipative steel cushions

Ghabraie et al. (2010) performed numerical shape optimization for steel slit damper. It was stated that bidirectional evolutionary structural optimization resulted in an increased energy dissipation capacity and low-cycle fatigue resistance of the damper. Zhang et al. (2017) proposed a twofold design method for coupling beam dampers to achieve optimum energy dissipation characteristics. The optimized dissipator had a simple geometry with high energy dissipation capacity.

Fallah and Honarparast (2013) investigated the optimal parameters for Pall friction dampers. Three objective functions were satisfied using a non-dominated sorting genetic algorithm. Base shear of a 10-story frame decreased considerably by the optimized dampers. Jarrahi et al. (2020) proposed an optimal design for the seismic control of inelastic systems with rotational friction dampers based on the seismic energy concept and particle swarm technique. Ratio of the seismic input energy to the dissipated energy was the objective function. Seismic capacities of the inelastic systems were found to be significantly increased by the optimal dampers.

Lavan and Daniel (2013) aimed using full resources of irregular structures through multiple tuned mass dampers (TMDs) with possible lowest mass. Comparisons with the gradient-based technique yielded that the developed process was almost optimal. Bilondi et al. (2018) evaluated four objective functions related with mass, stiffness, damping, and input energy to optimize TMDs. Optimization considering the cumulative hysteretic energy yielded the best results.

Liu and Shimoda (2013) improved deformation capability of a low-yield steel shear panel damper through shape optimization by performing finite element analyses. Equivalent plastic

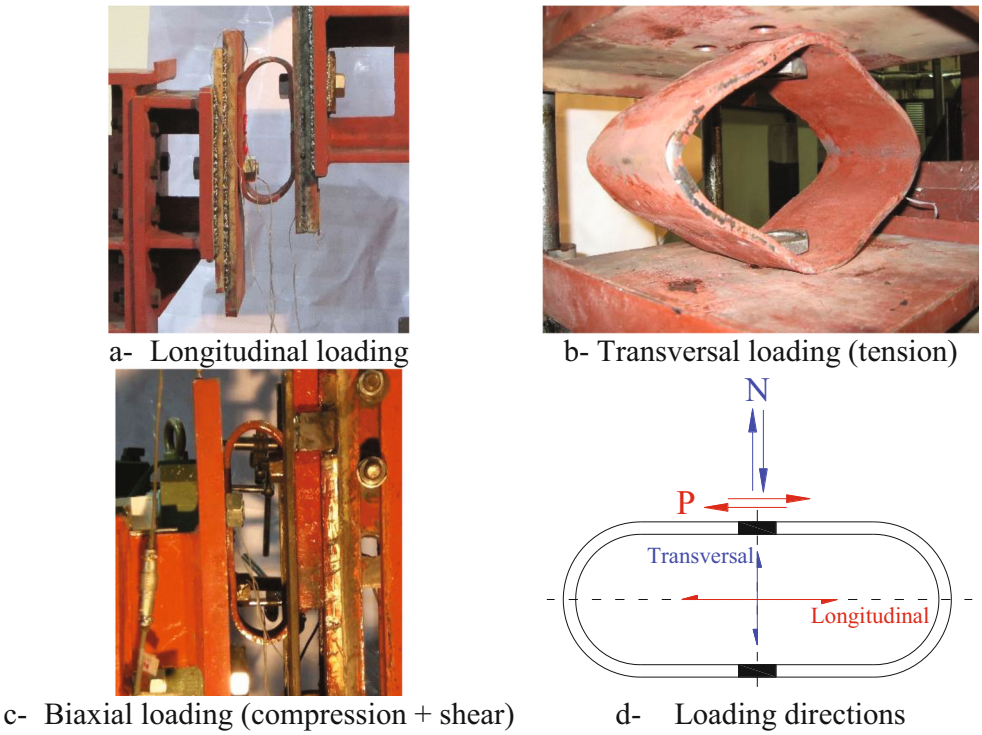

Fig. 2 **a**–**d** Performed experiments on the steel cushions

strain and total absorbed energy were considered as objectives. Plastic strain of the damper reduced to 82.2% by optimization.

Moeindarbari and Taghikhany (2014) performed numerical optimization based on genetic algorithms for optimum seismic design of triple friction pendulum bearing subjected to near-fault pulse-like ground motions. Ranges for design variables to achieve optimal performance were proposed in the study.

The aforementioned studies showed that optimized energy dissipative elements considerably reduced the base shear, story drifts, and plastic strains on structural members as well as increased the seismic energy dissipation capacity of structures. In these studies, objective functions based on seismic energy were found to be more competent (Liu and Shimoda 2013; Bilondi et al. 2018; Jarrahi et al. 2020). Therefore, energy-based objective functions are implemented to the optimization problem of SCs.

Steel cushions were proved to be significantly effective in enhancing seismic performance of the structures. However, the initial design of SC did not have the optimal dimensions that maximize its energy dissipative characteristics. So, the rationale of the study is enhancing energy dissipative characteristics of the steel cushion for longitudinal loading by optimal sizing. In the extent of the study, three distinct optimization techniques, namely sequential quadratic programming (SQP), gradient-based (GB) method, and Lagrange multiplier (LM) method, are utilized with three diverse objectives based on dissipated energy, cumulative dissipated energy, and equivalent damping ratio. Since the objective functions could be derived through closed form equations, the problem is converted to a mathematical problem from an engineering application. The optimally sized SCs are evaluated through experimentally verified finite element analyses.

2 Energy dissipative steel cushions

Energy dissipative steel cushions, produced by bending steel sheets, consist of two half circles and a straight part. Originally, SCs were fixed by using one thick bolt (Fig. 1a) whereas thinner two bolts were preferred to eliminate rotational movements in the improved design by Güllü et al. (2018) (Fig. 1b).

The in-plane hysteretic behavior of SCs was well-studied in the literature experimentally, numerically, and analytically for uniaxial (longitudinal *or* transversal) (Fig. 2a and b) and biaxial (longitudinal *and* transversal) (Fig. 2c) loadings (Ozkaynak et al. 2018; Yuksel et al. 2018). The transversal and longitudinal directions of SCs are depicted in Fig. 2d. The tested specimens had 150-mm straight part length, 50-mm radius, and 100-mm width. The thickness of the utilized steel sheets was 3, 5, and 8 mm.

All of the experiments resulted in almost ideal rectangular hysteretic behavior as a common property of metallic dampers. A hardening part was observed in the hysteresis when the inner surface of SC touched the nuts (Fig. 3).

The experimentally obtained results and observations yielded that SCs might be much more effective in the longitudinal direction. Equivalent damping ratios of SCs were experimentally determined to be about 50% and 18% for longitudinal and transversal loadings, respectively (Ozkaynak et al. 2018). Moreover, displacement capacity of SCs was the gap between the top and bottom nuts for the transversal loading, whereas it is equal to straight part length in case of longitudinal loading. Hence, they were utilized in the longitudinal direction to retrofit and/or enhance seismic behavior of distinct MDOF skeleton frames (Güllü 2018; Güllü et al. 2018).

Closed form design equations of yielding force (P_y), longitudinal displacement (δ_h), maximum moment ($M_{\max}$), and its location ($\varphi_{\max}$) for longitudinal loading were derived by using the flexibility method (1–4) (Ozkaynak et al. 2018). In the equations, i is $\sqrt{-1}$ and f_{yd} is yielding strength of the steel sheet. Longitudinal displacement (δ_h) corresponding to P_y is nominated as δ_y throughout the paper.

Other design variables are described in Fig. 4. It is worth noting that maximum displacement capacity of the SCs (δ_u) is equal to the straight part length of $2a$.

$$P_y = \frac{f_{yd} b t^2}{2r\cos\varphi_{\max}} \tag{1}$$

$$\delta_h = \int \frac{M\overline{M}}{EI} ds = \frac{Pr^2}{2EI}\left(\frac{5a^4 + 9\pi a^3 r + (36 + 1.5\pi^2)a^2 r^2 + 12\pi a r^3 + (2.25\pi^2 - 12)r^4}{4a^3 + 6\pi a^2 r + 24 a r^2 + 3\pi r^3}\right) \tag{2}$$

$$\varphi_{\max} = -\frac{1}{2}\ln\left(\frac{1.5\,i\pi r^3 + 12\,i a r^2 - 3a^2 r + 2\,i a^3 - 6r^3 - 3\pi a r^2 + 3\,i\pi a^2 r}{1.5\,i\pi r^3 + 12\,i a r^2 + 3a^2 r + 2\,i a^3 + 6r^3 + 3\pi a r^2 + 3\,i\pi a^2 r}\right) i \tag{3}$$

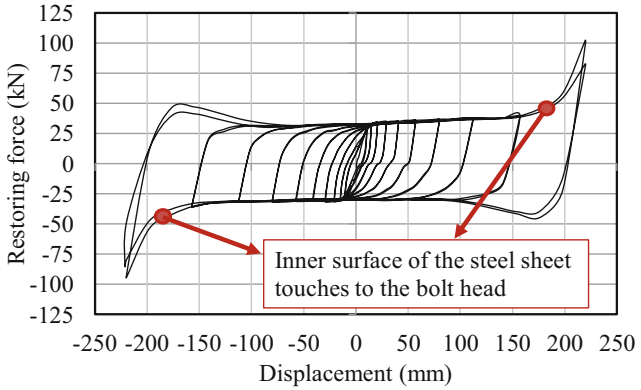

Fig. 3 Typical hysteresis of the steel cushions

$$M(\varphi) = \frac{\mathrm{Pr}}{2}(1-\cos\varphi) + \frac{a + r\sin\varphi}{a + r}\left[-\frac{Pr(a+r)(a^2+\pi ar+2r^2)}{4a^3/3+2\pi a^2 r+8ar^2+\pi r^3}\right] \quad (4)$$

3 Formulation of the constrained design optimization problem of SCs for longitudinal loading

Optimization is a practical tool to achieve finest performance of engineering applications. Current optimization techniques can be classified as local or global, constrained or unconstrained, continuous or discrete, gradient-based or non-gradient-based, as well as stochastic or deterministic (Nocedal and Wright 2006). Effective parameters for selection of the appropriate technique are based on the type of the optimization problem, quality of the desired solution, nature and availability of the algorithm, available computing sources, time constraints, existing software, etc. (Conn et al. 2000; Blum and Roli 2003; Yang 2010; Yang and Leifsson 2014). Several distinct algorithms like Newton, steepest descent, trust-region, gradient-based, sequential quadratic programming, and Lagrange multiplier methods can be performed for the problems with large number of design variables (Conn et al. 2000; Yang and Leifsson 2014).

The sequential quadratic programming (SQP) method is desirable for the non-linear problems, since it copes with any degree of non-linearity. SQP solves a number of subproblems that linearize each of the constraints to optimize a quadratic model of objective function (Nocedal and Wright 2006). Besides, the method was preferred in optimization problems where objective functions and constraints can be differentiated twice continuously (Gill et al. 1981; Powell 1983; Fletcher 1987). The method is equivalent to applying Newton's method to the first-order optimality conditions of the problem when the optimization problem has only equality constraints (Bonnas et al. 2006).

If the main goal of the optimization is to find a viable solution that might not be the best one, gradient-based (GB) methods can be preferred (Yang 2019). GB algorithm is based on the computation of gradients of the objective functions and the constraints with respect to the parameters which are used to solve the optimization problem.

Lagrange multiplier is preferred to solve the constrained optimization problems in many engineering applications (Bertsekas 2014). This method is an approach for finding the local maxima or minima of a function subject to equality/inequality constraints. Using the Lagrangian function, the original problem is rearranged by establishing the relationship between the gradient of the function and the gradients of the constraints (Lasdon 2002).

Considering the features of the above-mentioned optimization methods, the constrained multi-objective optimization

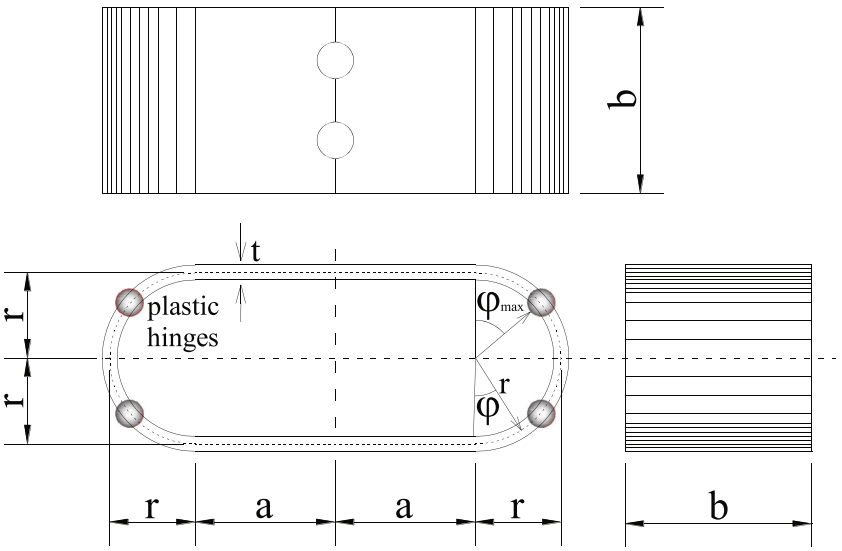

Fig. 4 Parameters utilized in the closed form solutions

problem is solved through SQP, GB, and LM with Hessian methods. The discrete objective functions of the optimization problem aimed at maximizing dissipated energy, cumulative dissipated energy by SC, and equivalent damping ratio of SC.

3.1 Optimization problem setting

The constrained multi-objective optimization problem subjected to (1–3) is defined in a mathematical form in (5) in which $\theta = [a, b, t, r]$is the parameter.

$$\begin{aligned} &\max\ \mathrm{F}(\theta) = [\mathrm{F}_1(\theta), \mathrm{F}_2(\theta), \mathrm{F}_3(\theta)] \\ &\mathrm{F}_1(\theta) = \text{Dissipated Energy}(\theta) \\ &\mathrm{F}_2(\theta) = \text{Cumulative Dissipated Energy}(\theta) \\ &\mathrm{F}_3(\theta) = \text{Equivalent Damping Ratio}(\theta) \end{aligned} \tag{5}$$

The objective functions to enhance longitudinal behavior of SCs are defined in the following sections.

3.1.1 Objective function for dissipated energy (F1)

Owing to derived closed form equations, an elastic perfectly plastic force-displacement curve of SCs can be constructed easily (Fig. 5).

Areas under the elastic and plastic parts of the curve are nominated as A_1 and A_2 in the figure which correspond to dissipated elastic and plastic energies. They can be formulated as given in (6a, 6b).

$$A_1 = \frac{1}{2} P_y \delta_y \tag{6a}$$

$$A_2 = P_y\left(\delta_u - \delta_y\right) \tag{6b}$$

In practical engineering, energy dissipators are expected to dissipate some part of seismic energy even during relatively lower level of shaking. Hence, minimizing the elastic energy or maximizing the plastic energy in the total energy (A_1+A_2) dissipated by SC is considered to be an object function (7).

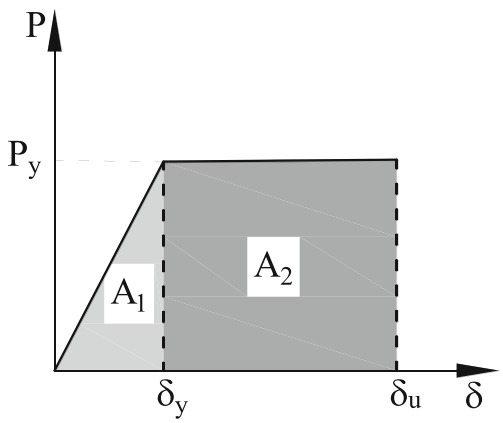

Fig. 5 Idealized force-displacement relation of SC

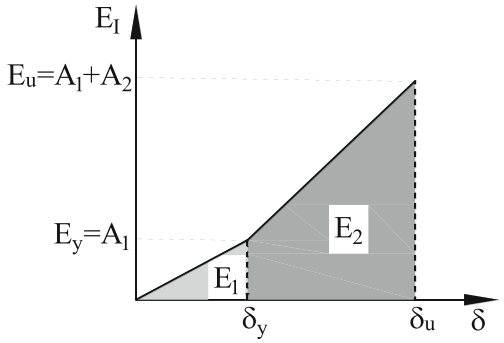

Fig. 6 Energy capacity curve of SC

$$\frac{A_2 - A_1}{A_2 + A_1} = \frac{2\delta_u - 3\delta_y}{2\delta_u - \delta_y} \tag{7}$$

3.1.2 Objective function for cumulative dissipated energy (F2)

Based on the obtained restoring force characteristics, energy capacity diagram of SCs can also be plotted (Fig. 6). Substantially, the energy capacity diagram represents dissipated energy by SC at a specific longitudinal displacement level. The first slope of the diagram corresponds to elastic energy while the second slope contains data about cumulative plastic energy.

Areas under the segments of the energy capacity curve (E_1 and E_2) can be calculated by (8a, 8b).

$$E_1 = \frac{1}{4} P_y \delta_y^2 \tag{8a}$$

$$E_2 = \frac{1}{2} P_y \delta_u \left(\delta_u - \delta_y\right) \tag{8b}$$

So, an object function aimed at maximizing E_2 (specifically increasing the second slope) is derived here to improve energy dissipation capacity of SCs (9).

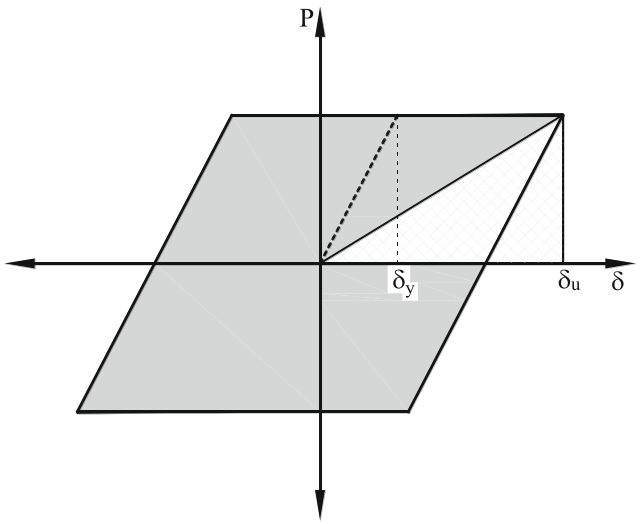

Fig. 7 Determination of the equivalent damping ratio of SC

$$\frac{E_2}{E_1} = \frac{2\delta_u(\delta_u - \delta_y)}{\delta_y^2} \tag{9}$$

3.1.3 Objective function for equivalent damping ratio (F3)

Damping ratio (ξ) of a hysteretic system can be calculated by (10) (Chopra 2001). In the equation, E_D and E_s stand for area of the hysteresis and the dashed triangle (see Fig. 7).

$$\xi = \frac{1}{4\pi}\frac{E_D}{E_s} \tag{10}$$

By substituting the areas E_D (area of the parallelogram) and E_s (area of the triangle) into (10), damping ratio of SC can be determined by (11). Hence, the object function aimed at maximizing the equivalent damping ratio of SC.

$$\xi_{SC} = \frac{2}{\pi}\frac{(\delta_u - \delta_y)}{\delta_u} \tag{11}$$

3.2 Application of the optimization techniques

The constraints of the non-linear multi-objective optimization problem (5) (C_1, C_2, and C_3) are given in (1–3) while the objectives F_1, F_2, and F_3 are given in (7), (9), and (11), respectively. The initial values for the variables are set to be the same with experimentally tested specimens.

The underlying idea of SQP is forming the optimization problem at an iterate x_k by a quadratic programming sub-problem and using a minimizer for this sub-problem to define a new iterate x_{k+1}. The interpretation is done in such a way that the sequence x_k converges to a local minimum x^* of the optimization problem as $k \to \infty$. Algorithm of the method is given in (12) for the optimization problem (5). In the equation, λ_1, λ_2, and λ_3 are Lagrange multipliers.

Table 1 Optimization results for design variables of SCs

Opt. algorithm	Obj. function	*a*/*r*	*b*/*t*	*a*/*b*
SQP	F1	4.76	20.00	1.90
	F2	4.61	20.00	1.88
	F3	4.75	20.00	1.91
GB	F1	2.74	20.00	1.59
	F2	2.76	20.00	1.56
	F3	2.74	20.00	1.59
LM	F1	3.09	20.00	1.10
	F2	3.02	20.00	1.14
	F3	3.20	20.00	1.07

$$L\{\theta, \lambda_1, \lambda_2, \lambda_3\} = F_i - \lambda_1 C_1 - \lambda_2 C_2 - \lambda_3 C_3, \mathrm{i} = 1, 2, 3 \tag{12}$$

A basic SQP algorithm defines an appropriate search direction d_k as a solution to the quadratic sub-problem at an iterate x_k (13a) which subjected to (13b).

$$\min_d \nabla F_i(\theta_k)^T d + \frac{1}{2} d^T \nabla^2_{xx} L\{\theta_k, \lambda_{1k}, \lambda_{2k}, \lambda_{3k}\} d \tag{13a}$$

$$C_i(\theta_k) + \nabla C_i(\theta_k)^T d = 0, \mathrm{i} = 1, 2, 3 \tag{13b}$$

Calculating the gradients of both constraints and objective functions is the first step for the GB algorithm. Since it is based on the gradients, the solution process is faster. Gradients of the distinct objective functions, $F_i(\theta)$, and the equality constraints, $C_i(\theta)$, are given in (14a, 14b).

$$\nabla F(\theta) = \begin{bmatrix} \frac{\partial F_1}{\partial a} & \frac{\partial F_2}{\partial a} & \frac{\partial F_3}{\partial a} \\ \frac{\partial F_1}{\partial b} & \frac{\partial F_2}{\partial b} & \frac{\partial F_3}{\partial b} \\ \frac{\partial F_1}{\partial t} & \frac{\partial F_2}{\partial t} & \frac{\partial F_3}{\partial t} \\ \frac{\partial F_1}{\partial r} & \frac{\partial F_2}{\partial r} & \frac{\partial F_3}{\partial r} \end{bmatrix} \tag{14a}$$

$$\nabla C(\theta) = \begin{bmatrix} \frac{\partial C_1}{\partial a} & \frac{\partial C_2}{\partial a} & \frac{\partial C_3}{\partial a} \\ \frac{\partial C_1}{\partial b} & \frac{\partial C_2}{\partial b} & \frac{\partial C_3}{\partial b} \\ \frac{\partial C_1}{\partial t} & \frac{\partial C_2}{\partial t} & \frac{\partial C_3}{\partial t} \\ \frac{\partial C_1}{\partial r} & \frac{\partial C_2}{\partial r} & \frac{\partial C_3}{\partial r} \end{bmatrix} \tag{14b}$$

The Lagrange multipliers used to augment the constraints to the functions are sometimes referred to an influence, or sensitivity functions that indicate how the objective function F_i is influenced by or sensitive to changes in the corresponding variables a, b, t, and r. An optimization problem might be solved more efficiently with a Hessian function, since it is possible to obtain faster and more accurate solutions. The Hessian of a Lagrangian function is given in (15) where F_1, F_2 , and F_3 are the objective functions; C_1, C_2, and C_3 are the non-linear equality constraints; and λ_1, λ_2, and λ_3 are associated Lagrange multipliers.

Table 2 Required function evaluation numbers for distinct optimization methods

Optimization algorithm	F1	F2	F3
SQP	213	173	149
GB	36	59	36
LM	125	40	112

Table 3 Smoothed geometric dimensions of optimized SCs

Optimization algorithm	a (mm)	b (mm)	t (mm)	r (mm)
SQP	38.0	20.0	1.0	8.0
GB	31.5	20.0	1.0	11.5
LM	22.0	20.0	1.0	7.0

$$\nabla^2 L\{\theta, \lambda_1, \lambda_2, \lambda_3\} = \nabla^2 F_i(\theta) - \sum \lambda_i \nabla^2 C_i(\theta), \mathrm{i} = 1, 2, 3 \quad (15)$$

Resultant geometric ratios (a/r, b/t, and a/b) of the SC for distinct optimization algorithms and objective functions are tabulated in Table 1. Additionally, required function evaluation numbers for all the studied algorithms and the objective functions are listed in Table 2.

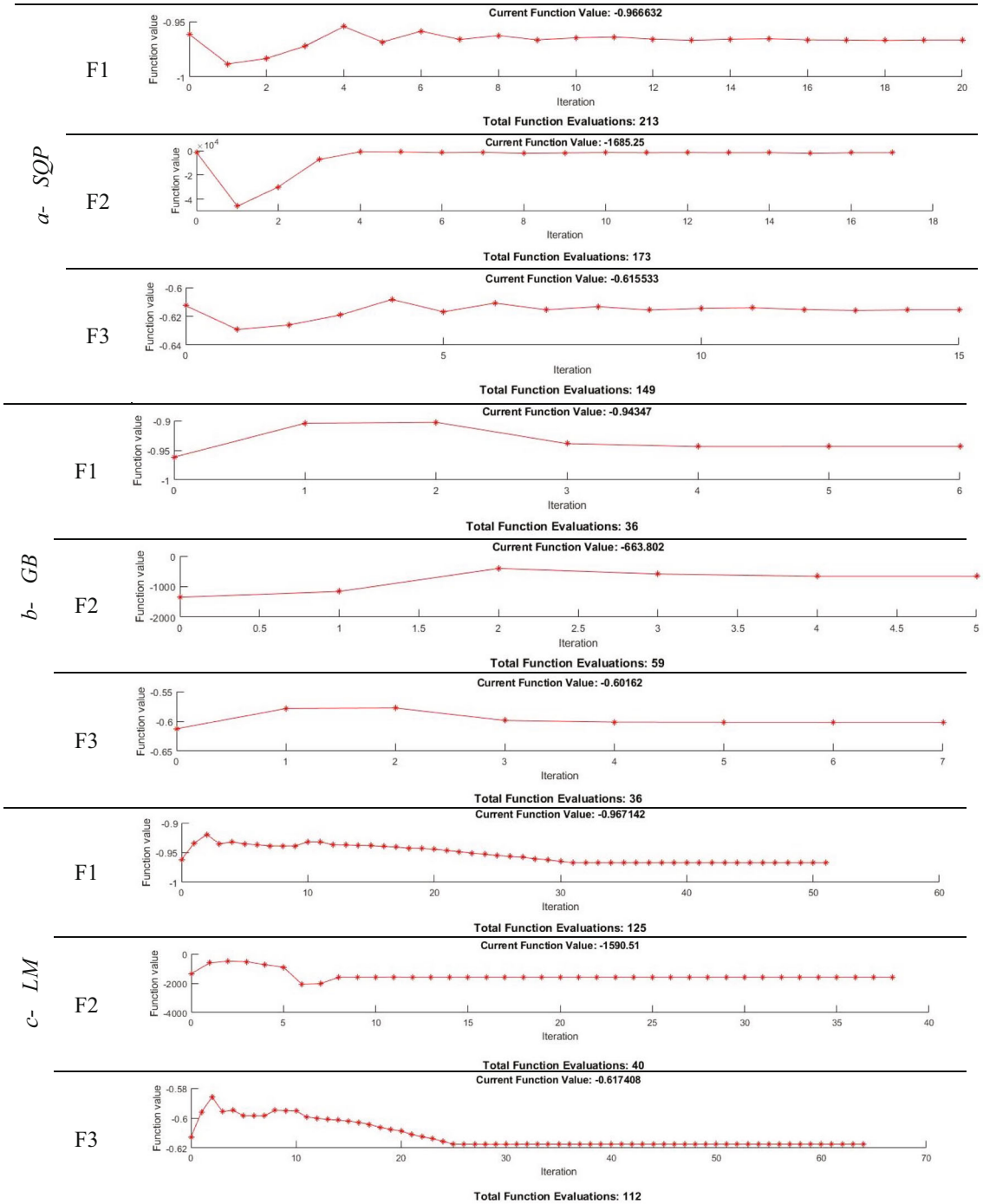

Fig. 8 Calculated object function values by each optimization method for the all objective functions

Table 4 Resultant object function values for each method

Optimization algorithm	Resultant object function value		
	F1	F2	F3
SQP	0.967	1685.250	0.616
GB	0.943	663.802	0.602
LM	0.967	1590.510	0.617

Each optimization method produced similar results for the distinct object functions. Therefore, the ratios are smoothed to an average value. The smoothed dimensions of optimized SCs, those utilized for the numerical assessments, are given in Table 3. By assuming $t = 1$ mm, other variables given in the table are obtained through the optimal geometric ratios.

Comparing the optimization results (i.e., optimized function value) obtained with the Lagrange multiplier including a Hessian with others shows that the method is superior in finding optimal solutions and shows significant accuracy and reasonable convergence in achieving optimal values. Optimized function values against evaluated function numbers are plotted in Fig. 8 for all the methods.

The gradient-based method takes fewer function evaluations and works accurately. However, greater object function values are obtained by the Lagrange multiplier method with a Hessian. The resultant object function values are given in Table 4 for each optimization method. When three different methods and three discrete objective functions are compared, it can be concluded that including a gradient to the optimization method results in fewer iterations to solve the optimization problem.

Efficiency and accuracy of the utilized optimization methods (SQP, GB, and LM) are evaluated by a metaheuristic method, namely genetic algorithm (GA). Optimization methods might be classified as deterministic or stochastic. A problem may be called deterministic if there is no randomness in the formulation. The stochastic methods have also two branches as heuristic and metaheuristic algorithms. One of the contemporary trends is to apply intelligent algorithms that are also known as metaheuristic or evolutionary to solve the optimization problems since traditional methods are insufficient in finding global optimal values. Moreover, there is a tendency to call all stochastic algorithms as metaheuristic algorithm using randomization and local search. Metaheuristic algorithms can also be classified in many different ways. GA is a population-based algorithm as they use a set of strings (Yang 2018).

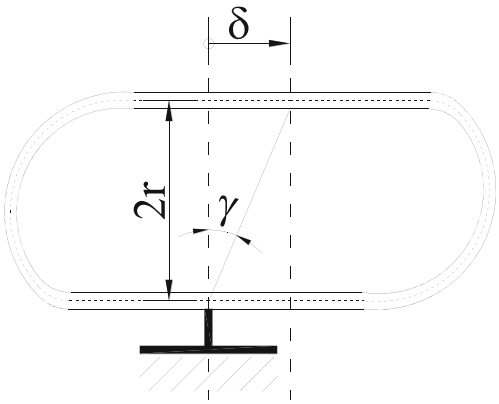

Fig. 10 Deformed SC and definition of shear angle γ

GA works in the same way of the evolutionary process observed on a biological natural selection. Evolution usually starts from a population of randomly generated individuals. It is an iterative process in which the population in each iteration is called one generation. Instead of developing a single structure for the solution as in other optimization methods, it forms a cluster of such structures. Representing many possible solutions to the problem, this cluster is called population in genetic algorithm terminology. The algorithm repeatedly changes a population of individual solutions. This algorithm randomly selects individuals from the population present at each step. Then, they are used as parents to produce future generations. As the generations come one after another, the population evolves towards an optimal solution (Beasley et al. 1993). GA can be applied to solve non-linear, stochastic, discontinuous problems that are not very suitable for standard optimization algorithms.

When the GA is utilized for the solution of the optimization problem (5), the geometric ratios for a/r, b/t, and a/b are obtained to be 3.000, 20.000, and 1.216. The resultant ratios are quite consistent with the results of the LM method. Hence, efficiency and accuracy of the LM method are proven by means of an intelligent optimization technique. Moreover, resultant function values of GA are 0.925, 357.398, and 0.591, respectively. They are slightly below the results obtained with the LM method (see Table 4).

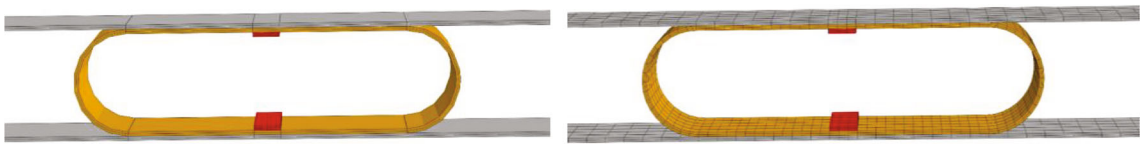

a- Model b- Meshing

Fig. 9 **a**, **b** A demonstrative FEM of SC

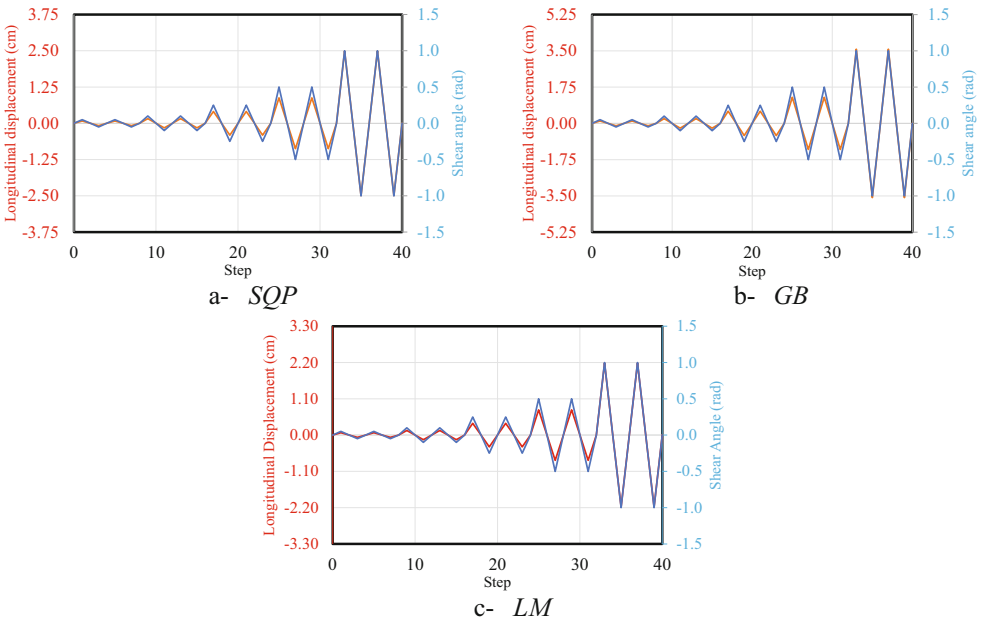

Fig. 11 **a**–**c** Loading schemes for optimized SCs

4 Numerical verification

Steel cushion is placed between two rigid walls in the finite element models (FEMs) which are generated by using ABAQUS v. 6.14 (2014). Fasteners are also implemented into the model (Güllü et al. 2019). A demonstrative rendered FEM and its meshing are illustrated in Fig. 9.

Two-dimensional and four-node S4R quadrilateral shell elements are utilized to increase accuracy of the finite element analyses while decreasing the computational effort. S4R utilizes the reduced integration technique and has hourglass control to avoid deceptive solutions to occur due to shear locking and hourglass shape. Moreover, five thickness integration points are used for the shell elements.

Surface-to-surface contacts (*interaction*) that have "*hard contact*" as normal behavior and "*penalty*" as tangential behavior between the rigid walls and SC as well as SC and fasteners are applied. The friction coefficient is assigned to be 0.6 since neither SC nor the *rigid walls* are lubricated in real applications.

Bottommost and uppermost surfaces of FEMs are coupled to reference points by using kinematic coupling property.

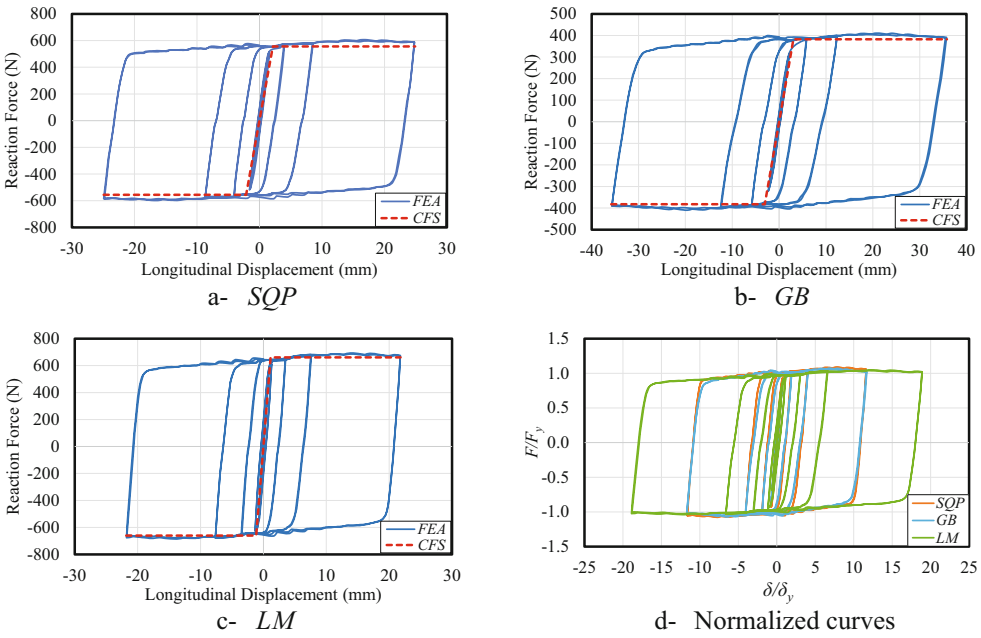

Fig. 12 **a**–**d** Obtained hysteresis for optimally sized SCs with different methods

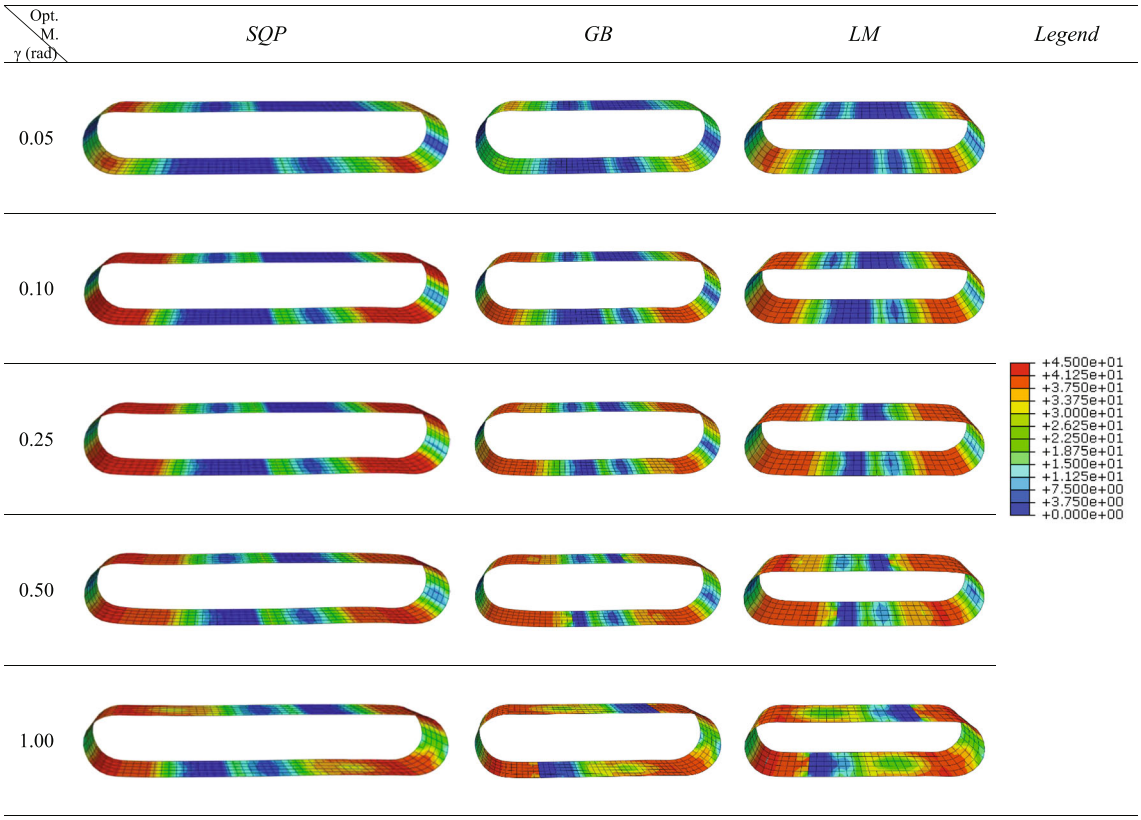

Fig. 13 von Mises stress distribution on the optimized SCs

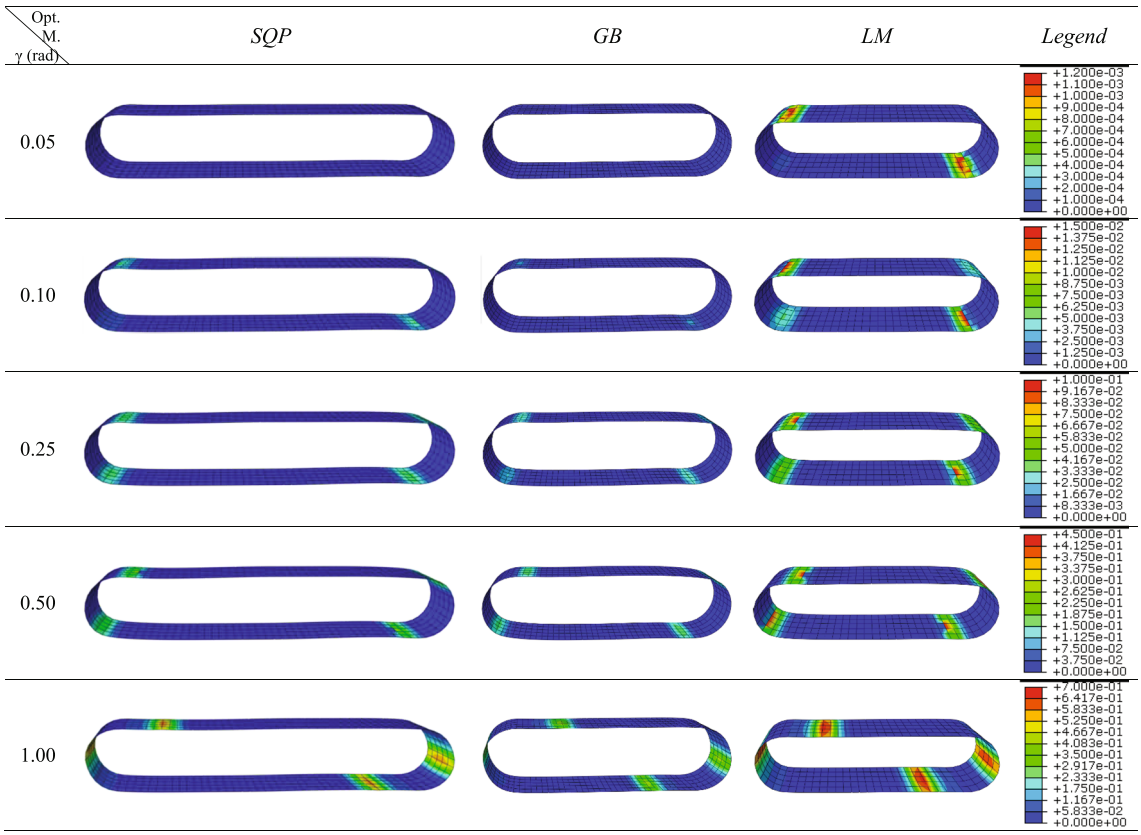

Fig. 14 PEEQ distribution on the optimized SCs

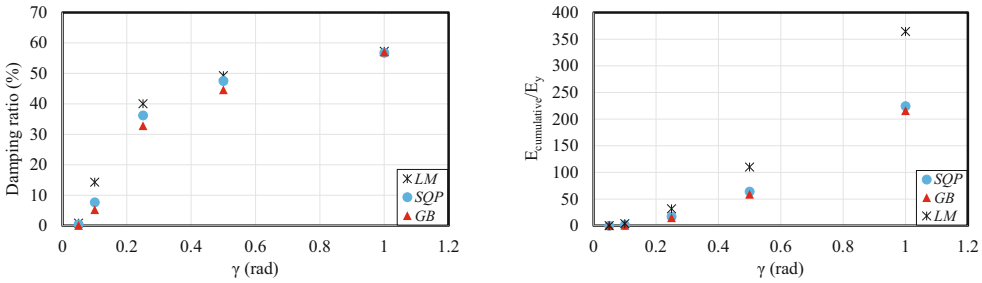

Fig. 15 **a**, **b** Energy dissipative characteristics of optimally sized SCs

Displacement of the bottom reference point is restricted (fix support) while the upper one forced to cyclic longitudinal displacement.

Coupon test results of Güllü et al. (2019) are adapted to the models with Poisson ratio of 0.3. Inelastic behavior of the steel is simulated by kinematic hardening in which relocation of the yielding surface origin is calculated by (16). In the equation, α is the back stress tensor, $\dot{\bar{\xi}}^{pl}$ and α_k are the incremental changes in the equivalent plastic strain and back stress tensor, respectively, and, γ_k and C are material parameters.

$$\dot{\alpha}_k = C_k \frac{1}{\sigma^0}(\sigma - \alpha)\dot{\bar{\xi}}^{pl} - \gamma_k \alpha_k \dot{\bar{\xi}}^{pl} \tag{16}$$

The direct Newton-Raphson method with linear increments between the adjacent steps is preferred for the solver.

Loading schemes to be applied to the optimally sized SCs are determined through shear angle (γ) which is depicted in Fig. 10.

SCs are exposed to two cycles for each shear angle level of 0.05, 0.10, 0.25, 0.50, and 1.00 rad. Corresponding displacements (δ) can be calculated by (17) which mainly depends on the radius (r) of the half circles. Since the models generated for the different optimization methods have varied radiuses, they are exposed to different levels of longitudinal displacement (Fig. 11).

$$\delta = 2r \times \tan(\gamma) \tag{17}$$

Initially, the resulting force-displacement hysteresis of the models is compared with the predictions of closed form solution (CFS) obtained by (1–4) in Fig. 12a–c. It is obvious that CFSs satisfactorily enveloped the hysteresis of SCs. Yielding displacements are obtained to be 2.136, 3.050, and 1.152 mm for SCs optimized by the SQP, GB, and LM methods, respectively. Corresponding yielding forces are 555.6, 382.4, and 660.4 N. The curves are normalized with their own yielding displacements and yielding forces to compare with each other (Fig. 12d). The normalized hysteresis of SCs optimized by SQP and GB methods is exactly the same while the LM method results in much more displacement ductility.

von Mises stress distributions and equivalent plastic strains (PEEQ) on the optimized SCs are shown in Figs. 13 and 14 for each shear angle level. All SCs experienced excessive stresses and plastic deformations around the connection edge of the circular and the straight parts. Maximum stresses obtained at the end of the analyses are 43.74, 42.46, and 45.25 kN/cm^2 for SCs optimally sized through SQP, GB, and LM methods, respectively, whereas maximum PEEQ intensities are attained to be 0.605, 0.442, and 0.678, respectively. SC optimally sized by GB exhibited prominently lower level of strains and stresses, whereas the one optimized with LM is exposed to highest plastic strains.

Hereafter, damping ratios and cumulative dissipated energy to the yielding energy ratios of the optimally sized SCs with distinct methods are calculated and compared in Figs. 15a, b. Damping ratio of SC is increased up to 58% from 50% by the optimization methods. In general, SC optimized with the LM method has greater equivalent damping ratio and cumulative plastic energy to yielding energy ratio ($E_{\text{cumulative}}/E_{\text{yield}}$). Total cumulative energies dissipated by the optimally sized SCs are 133.083 J, 125.826 J, and 138.600 J for SQP, GB, and LM methods, respectively.

Performed analyses showed that if SC were optimized by LM, it will require lower seismic energy to reach yielding point. Alternatively, SC may reach yielding points at lower reaction forces and reduced plastic deformations when it will be sized by the GB method.

5 Conclusions

In this study, multi-objective optimal sizing of energy dissipative steel cushion problem is solved by different methods. The objective functions, those optimized discretely, are the mathematical models of the dissipated energy, cumulative dissipated energy, and equivalent damping ratio. The following conclusions can be derived from the study.

For optimization procedure:

- Solutions obtained using the gradient-based method required fewer function evaluations with reasonable function values.
- The considered object functions resulted in quite similar values within each optimization method.

- Gradient-based and Lagrange multiplier methods reached almost similar values.
- The Lagrange multiplier method with Hessian converges more accurately compared to others with greatest function values.
- The utilized intelligent technique (genetic algorithm) proved the efficiency and accuracy of the Lagrange method since it yielded similar results.

For energy dissipative steel cushion:

- Smoothed geometric ratios of SC, namely a/r, b/t, and a/b, should be 3, 20, and 1.1, respectively. One can design a SC simply by considering provided optimal ratios and geometric restrictions in main structure, e.g., beam width (related to b), possible maximum height for the implementation of SC (related to $2r$).
- SC optimally sized by the Lagrange multiplier method with a Hessian has better energy dissipative characteristics.
- Equivalent damping ratios of the all models are increased up to 58% from 50% by optimal sizing.

Compliance with ethical standards

Conflict of interest The authors declare that they have no conflict of interest.

Replication of results All the data underlying the argument in the article are generated by locally developed MATLAB codes consisting of a set of systematically arranged sub-modules. We are willing to satisfy the reasonable and responsible demand for the data and the source codes underpinning the present article.

References

ABAQUS, v. 6.14 (2014) Computer software, Simulia, Dassault Systemes, Providence, RI, USA

Aiken I (1996) Passive energy dissipation – hardware and applications. In. Proc. SEAOSC Symposium on Passive Energy Dissipation Systems for New and Existing Buildings, Los Angeles, CA

Beasley D, Dr B, Martin RR (1993) An overview of genetic algorithms: part 1, fundamentals. University Computing 15(2):58–69

Bertsekas DP (2014) Constrained optimization and Lagrange multiplier methods. Academic press, London

Bilondi MRS, Yazdani H, Khatibinia M (2018) Seismic energy dissipation-based optimum design of tuned mass dampers. Struct Multidiscip Optim 58:2517–2531

Blum C, Roli A (2003) Metaheuristics in combinatorial optimization: overview and conceptual comparison. ACM Comput Surv 35(3): 268–308

Bonnas JF et al (2006) Numerical optimization: theoretical and practical aspects. Springer Science and Business Media, USA

Chopra A (2001) Dynamics of structures: theory and applications to earthquake engineering, 2nd edn. Pearson Prentice Hall, Pearson Education Inc., Upper Saddle River

Colombo A, Lamperti MT, Negro P, Toniolo G (2016) Design guidelines for wall panel connections. Edited by European Union. https://doi.org/10.2788/546845

Conn AR, Gould NIM, Toint PL (2000) Trust-region methods, MPS/SIAM series on optimization, SIAM and MPS. Society for Industrial and Applied Mathematics, Philadelphia

Dal Lago B, Biondini F, Toniolo G (2017) Friction-based dissipative devices for precast concrete panels. Eng Struct 147:356–371

Fallah N, Honarparast S (2013) NSGA-II based multi-objective optimization in design of Pall friction dampers. J Constr Steel Res 89:75–85

Fletcher R (1987) Practical methods of optimization. John Wiley and Sons, New York

Ghabraie K, Chan R, Huang X, Xie YM (2010) Shape optimization of metallic yielding devices for passive mitigation of seismic energy. Eng Struct 32:2258–2267

Gill PE, Murray W, Wright MH (1981) Practical optimization. Academic Press, London

Güllü A (2018) Determination of the inelastic displacement demand and response control of steel frame type structures by seismic energy equations. PhD Dissertation, Istanbul Technical University, Istanbul, Turkey

Güllü A, Yüksel E, Yalcin C (2018) Seismic energy based design: numerical evaluations of diverse MDOF systems. In. Proc. 16th European Conference on Earthquake Engineering, Thessaloniki, Greece

Güllü A, Smyrou E, Khajehdehi A, Ozkaynak H, Bal IE, Yuksel E, Karadogan F (2019) Numerical modelling of energy dissipative steel cushions. Int J Steel Struct 19(4):1331–1341

Jarrahi H, Asadi A, Khatibinia M, Etedali S (2020) Optimal design of rotational friction dampers for improving seismic performance of inelastic structures. J Build Eng 27:100960

Karadoğan F, Yüksel E, Khajehdehi A, Özkaynak H, Güllü A, Senol E (2019) Cyclic behavior of reinforced concrete cladding panels connected with energy dissipative steel cushions. Eng Struct 189:423–439

Lasdon LS (2002) Optimization theory for large systems. Mineola, New York

Lavan O, Daniel Y (2013) Full resources utilization seismic design of irregular structures using multiple tuned mass dampers. Struct Multidiscip Optim 48:517–532

Liu Y, Shimoda M (2013) Shape optimization of shear panel damper for improving the deformation ability under cyclic loading. Struct Multidiscip Optim 48:427–435

Moeindarbari H, Taghikhany T (2014) Seismic optimum desing of triple friction pendulum bearing subjected to near-fault pulse-like ground motions. Struct Multidiscip Optim 50:701–716

Nocedal J, Wright S (2006) Numerical optimization. USA, New York

Ozkaynak H (2018) Earthquake behavior of steel cushion-implemented reinforced concrete frames. Earthq Eng Eng Vib 17:385–401

Ozkaynak H, Gullu A, Gokce T, Khajehdehi A, Mahdavi M, Azizisales F, Bal IE, Smyrou E, Yuksel E, Karadogan F (2014) Energy dissipative steel cushions. In. Proc. 2nd European Conference on Earthquake Engineering and Seismology, Istanbul, Turkey

Ozkaynak H, Khajehdehi A, Gullu A, Azizisales F, Yuksel E, Karadogan F (2018) Uni-axial behavior of energy dissipative steel cushions. Steel Compos Struct 27(6):661–674

Powell MJD (1983) Variable metric methods for constrained optimization. In: Mathematical Programming: The State of the Art. Springer, Berlin

Sadek F, Mohraz B, Taylor AW, Chung RM (1996) Passive energy dissipating devices for seismic applications. Report No 5923, Building and Fire Research Laboratory, National Institute of Standards and Technology, Gaithersburg, Maryland

Safecladding FP7 Project (2012–2015) Improved fastening systems of cladding panels for precast buildings in seismic zones

Sonmez M, Aydin E, Karabork T (2013) Using an artificial bee colony algorithm for the optimal placement of viscous dampers in planar building frames. Struct Multidiscip Optim 48:395–409

Soong TT, Spencer BF Jr (2002) Supplemental energy dissipation: state-of-the-art and state-of-the-practice. Eng Struct 24:243–249

Soydan C, Yuksel E, Irtem E (2014) The behavior of a steel connection equipped with the lead extrusion damper. Adv Struct Eng 17(1):25–39

Soydan C, Yuksel E, Irtem E (2018) Retrofitting of pinned beam–column connections in RC precast frames using lead extrusion dampers. Bull Earthq Eng 16(3):1273–1292

Soydan C, Yüksel E, İrtem E (2020) Seismic performance improvement of single-storey precast reinforced concrete industrial buildings in use. Soil Dyn Earthq Eng 135:106167

Yang XS (2010) Engineering optimization: an introduction with metaheuristic applications. John Wiley and Sons, USA

Yang XS (2018) Optimization techniques and applications with examples. John Wiley and Sons, USA

Yang XS (2019) Introduction to algorithms for data mining and machine learning. Academic Press, London

Yang XSK, Leifsson SL (2014) Computational optimization, modelling and simulation: past, present and future. Procedia Comput Sci 29: 754–758

Yuksel E, Karadogan F, Ozkaynak H, Khajehdehi A, Güllü A, Smyrou E, Bal IE (2018) Behaviour of steel cushions subjected to combined actions. Bull Earthq Eng 16(2):707–729

Zhang Z, Qu J, Li D, Zhang S (2017) Optimization of coupling beam metal damper in shear wall structures. Appl Sci 7:137

Zhou L, Wang X, Ye A (2019) Low cycle fatigue performance investigation on transverse steel dampers for bridges under ground motion sequences using shake-table tests. Eng Struct 196:109328